Electronic Supplementary Material (ESI) for ChemComm.

Supporting Information

Two high-nuclearity isopolyoxoniobates containing $\{Nb_{54}O_{151}\}$-based helical nanotubes for the decomposition of chemical warfare agent simulants

Yan-Lan Wu, Yong-Jiang Wang, Yan-Qiong Sun*, Xin-Xiong Li and Shou-Tian Zheng *

State Key Laboratory of Photocatalysis on Energy and Environment, College of Chemistry, Fuzhou University, Fuzhou, Fujian 350108, China.

E-mail: *sunyq@fzu.edu.cn; stzheng@fzu.edu.cn;*

Contents

Section S1: Experiments and Methods

1. Material and general methods

All chemicals were commercially purchased and used without further purification. $K_7HNb_6O_{19}\cdot 13H_2O$ was prepared according to the literature and identified by IR spectrum.[S1] IR spectra were determined in the range 4000-400 cm^{-1} on a Nicolet IS50 Fourier transform infrared (FT/IR) spectrometer. ICP analyses were conducted on an Ultima2 spectrometer. XPS analyses were conducted on a Thermo Scientific Nexsa. ^{31}P NMR (202.46 MHz) spectroscopy conducted on an AVANCE III 400 MHz spectrometer, was used to detect the reagents and products from the catalytic reactions. Samples were placed in 5 mm O.D. NMR tubes and chemical shifts were referenced to H_3PO_4 (taken as 0 ppm at 25 °C). PXRD patterns were obtained by using an Ultima IV diffractometer with Cu-Kα radiation (λ = 1.5418 Å) in the range 5-50 °. Thermogravimetric analyses were conducted using a Mettler Toledo TGA/SDTA 851^e analyzer in an N_2-flow atmosphere with a heating rate of 10 °C/min at a temperature of 30-800 °C. UV-vis spectra were performed on a SHIMADZU UV-2600 UV-visible spectrophotometer by using the $BaSO_4$ as the blank.

2. Syntheses and Synthetic discussion

(1) Synthesis of $H_5Na_7K_4[Cu(en)_2]_2[Cu(en)(H_2O)]_2[Cu(en)_2(H_2O)]_4[Nb_{54}O_{151}]\cdot 27H_2O$ (1).

A mixture of $K_7HNb_6O_{19}\cdot 13H_2O$ (0.665 g, 0.485 mmol), $NaHCO_3$ (0.405 g, 4.82 mmol), $Cu(CH_3COO)_2\cdot H_2O$ (0.086 g, 0.431 mmol), $Li_2B_4O_7$ (0.049 g, 0.290 mmol), 0.05 mL en was mixed in 10 mL H_2O. After stirred 1 hour, the resulting mixture was sealed in a Teflon-lined autoclave (23 mL) and heated at 200 °C for 5 days. After cooling down, the filtrate was kept at room temperature for about one week and light purple crystals were obtained. Yield: 70 mg (13.6 %, based on Nb). The pH values before and after reaction were ca. 9.5 and 9.0, respectively. Elemental analysis (based on dried sample) calcd (found) % for $H_{183}Na_7K_4Cu_8C_{28}N_{28}Nb_{54}O_{184}$: Na, 1.66 (1.68); Cu, 5.24 (5.30); K, 1.61 (1.63); Nb, 51.72 (52.33). IR (KBr, cm^{-1}): 3248(m), 1629(s), 1418(s), 1109(m), 1036(m), 912(s), 846(w), 831(s), 752(w), 656(s), 562(s), 496(w).

(2) Synthesis of $H_3Na_4K_3[Cu(H_2O)_3][Cu(en)_2]_2[Cu(en)(H_2O)]_4[Cu(en)_2(H_2O)]_4[Nb_{54}O_{151}]\cdot 22H_2O$ (2).

A mixture of $K_7HNb_6O_{19}\cdot 13H_2O$ (0.655 g, 0.478 mmol), $NaHCO_3$ (0.4 g, 4.76 mmol), $Cu(CH_3COO)_2\cdot H_2O$ (0.088 g, 0.441 mmol), $Li_2B_4O_7$ (0.05 g, 0.296 mmol), 0.05 mL en was mixed in 10 mL H_2O, After stirred 1 hour, the resulting mixture was sealed in a Teflon-lined autoclave (23 mL) and heated at 160 °C for 5 days. After cooling to room temperature, light purple crystals were obtained. Yield: 25 mg (4.75 %, based on Nb). The pH values before and after reaction were ca. 9.6 and 9.0, respectively. Elemental analysis (based on dried sample) calcd (found %) for $H_{197}Na_4K_3Cu_{11}C_{32}N_{32}Nb_{54}O_{184}$: Na, 0.93 (0.94); Cu, 7.06 (7.15); K, 1.18 (1.20); Nb, 50.68 (51.34). IR (KBr, cm^{-1}): 3238(m), 1641(s), 1576(s), 1364(m), 1160(w), 1101(w), 1036(s), 912(s), 861(s), 825(w), 744(s), 569(s), 469(w).

(3). Synthetic Discussion

In this work, we found that the following reaction parameters show important impacts on the syntheses:

(1) The temperature of hydrothermal reactions is one of the important factors for the syntheses of compounds **1** and **2**. The mixture raw materials of compound **1** reacted in 200 °C high temperature, and then the reaction products were filtrated. The crystals of compound **1** were obtained by evaporating the filtrate at room temperature for about one week, while compound **2** was obtained in lower temperature 160 °C. When the reaction is higher or lower than the specific temperature, the yield would decrease dramatically and only amorphous phases would be obtained.

(2) We synthesized two compounds in H_2O in presence of en, when we changed the solvent to other buffer solutions, such as $Na_2CO_3/NaHCO_3$ and $Na_2B_4O_7/H_3BO_3$, or changed the en to other organic-ammines, none of them would be obtained in the reaction.

(3) We have further explored different synthetic methods to improve the yield of the products, for example adjusting the reactant ratio, reaction time, pH values of the reaction. We have modulated the reaction ratio about raw materials of compound **1**, the crystals would be obtained as the mass of $Cu(CH_3COO)_2\cdot H_2O$ was 0.1g, but the yield of product was low. When we further increased or decreased the mass of $Cu(CH_3COO)_2\cdot H_2O$, the product of **1** could not be obtained. When we did the same investigation of compound **2**, we would not obtain the products of **2**. To lengthen or shorten the reaction time to 120 min, 90 min, 45 min, 40 min, 15 min, 2 min for compounds **1** and **2**, we could not obtain both of them under the hydrothermal reaction or with a solvent evaporation method at room temperature. When we adjusted the pH of buffer solution, a lot of amorphous phases would be obtained. When we adjust the quantity of solvent and alkaline metal salts, we could not obtain

samples as well and all of these investigations may probably suggest the reaction conditions of compounds **1** and **2** are harsh. So the yields for compounds **1** and **2** were low.

3. Single–crystal X-ray Crystallography

Crystals were collected on a Bruker APEX Due CCD area diffractometer equipped with a fine focus, 2.0 kW sealed tube X-ray source (MoKα radiation, λ = 0.71073 Å) operating at 175(2) K. The empirical absorption correction was based on equivalent reflections. Structures were solved by direct methods followed by successive difference Fourier methods. Computations were performed using SHELXTL and final full-matrix refinements were against F^2.[S2] The contribution of disordered solvent molecules to the overall intensity data of structures were treated using the SQUEEZE method in PLATON, and the details of squeeze have been included in the end of CIF files of two compounds, and we can see that the disordered atoms in void are less than 3.91 eA^{-3}, suggesting that they are reasonable to use Squeeze method. CCDC 2105822-2105823 contain the supplementary crystallographic data for compounds **1** and **2**, respectively.

4. Supplementary Physical Characterization

(1) Degradation of DMMP by compound 1

In a typical reaction, 50 mg of compound **1**, DMMP (2.5 μL) and D_2O (0.6 mL) were mixed with 1.0 mL of deionized water in a 2-mL scintillation vial. This mixture was vigorously stirred at room temperature. Every several hours, a 400 μL aliquot of the solvent was transferred into the NMR tube for ^{31}P NMR measurement; the aliquot was then transferred back to the vial for further reaction. After 264 hours, the solid was collected by centrifugation, washed extensively with mother liquid of compound **1** and dried. The resulting solid was then characterized by FT-IR.

(2) Degradation of DECP by compound 1

In a typical reaction, 30 mg of compound **1** was suspended in 600 μL of DMF placed in a 5-mL O.D. NMR tube. Subsequently, 10 μL of DECP and 50 μL of H_2O were added. The mixture was vigorously shaken at room temperature. Every 5 minutes, the contents were assessed by ^{31}P NMR spectroscopy to monitor the reaction. After the DECP has been completely hydrolyzed, the solid was collected by centrifugation, washed extensively with mother liquid of compound **1** and dried. The resulting solid was then characterized by FT-IR and XRD.

Section S2 Additional Tables

Table S1 Crystal Data and Structure Refinements for 1-2.

Compound	1	2
Empirical formula	$H_{183}Na_7K_4Cu_8C_{28}N_{28}Nb_{54}O_{184}$	$H_{197}Na_4K_3Cu_{11}C_{32}N_{32}Nb_{54}O_{184}$
M	9699.80	9900.54
T/K	175(2)	175(2)
Crystal system	Orthorhombic	Orthorhombic
Space group	*Cmca*	*Cmca*
a/Å	56.364(3)	56.743(3)
b/Å	20.1214(12)	19.9065(10)
c/Å	51.165(3)	55.091(2)
α/°	90	90
β/°	90	90
γ/°	90	90
V/Å^3	58027(6)	62229(5)
Z	8	8
D_c/Mg m^{-3}	2.221	2.114
μ/mm^{-1}	2.769	2.765
F(000)	36944	37752
Data/restraints/parameters	25893 / 12 / 1284	27793 / 8 / 1334
$R_1(I > 2\sigma(I))$ [a]	0.0808	0.0679
wR_2 (all data) [a]	0.2405	0.1933
Goodness-of-fit on F^2	1.064	1.026

[a] $R_1 = \sum||F_0|-|F_C||/\sum|F_0|$; $wR_2 = \sum[w(F_0^2-F_C^2)^2]/\sum[w(F_0^2)^2]^{1/2}$

Table S2 Bond lengths and valence band summations of copper atoms in 1.

Atom1	Atom2	Rij	Ro	B	Sij	SUM
Cu1	N4	1.9628	1.61	0.4	0.413954	
	N3	2.0155	1.61	0.4	0.362856	
	N5	2.0156	1.61	0.4	0.362765	
	N6	2.0338	1.61	0.4	0.346629	
	O65	2.467	1.65	0.4	0.129704	
	OW9	2.626	1.65	0.4	0.087161	1.703069
Cu2	N14	1.9397	1.61	0.4	0.438564	
	N7	1.9876	1.61	0.4	0.389068	
	N1	2.0461	1.61	0.4	0.336132	
	N8	2.1455	1.61	0.4	0.262173	
	O56	2.542	1.65	0.4	0.107528	
	O48	2.674	1.65	0.4	0.077305	1.610771
Cu3	N11	1.9608	1.61	0.4	0.416029	
	N10	2.0078	1.61	0.4	0.369908	
	N12	2.0233	1.61	0.4	0.355849	
	N9	2.026	1.61	0.4	0.353455	

	OW7	2.629	1.65	0.4	0.08651	
	O50	2.575	1.65	0.4	0.099013	1.680764
Cu4	N13	1.9756	1.61	0.4	0.400917	
	N13	1.9756	1.61	0.4	0.400917	
	O5	2.0172	1.65	0.4	0.399317	
	O5	2.0172	1.65	0.4	0.399317	
	O1W	2.3748	1.65	0.4	0.163327	1.763796
Cu5	O20	1.9802	1.65	0.4	0.438016	
	O20	1.9802	1.65	0.4	0.438016	
	N2	1.9929	1.61	0.4	0.383947	
	N2	1.9929	1.61	0.4	0.383947	
	O2W	2.3744	1.65	0.4	0.163491	1.807417

Table S3 Bond lengths and valence band summations of protonated oxygens in 1.

Atom1	Atom2	Rij	Ro	B	Sij	SUM
O59	Nb16	1.8102	1.921	0.319	1.41529	1.41529

Table S4 Bond lengths and valence band summations of copper atoms in 2.

Atom1	Atom2	Rij	Ro	B	Sij	SUM
Cu1	N6	2.0009	1.61	0.4	0.376345	
	N7	2.0023	1.61	0.4	0.37503	
	N8	2.0169	1.61	0.4	0.361588	
	N5	2.0308	1.61	0.4	0.349239	
	O42	2.4284	1.65	0.4	0.142844	
	O77	2.707	1.65	0.4	0.071183	1.676228
Cu2	N2	2.0152	1.61	0.4	0.363128	
	N1	2.0188	1.61	0.4	0.359874	
	N4	2.0242	1.61	0.4	0.355049	
	N3	2.0286	1.61	0.4	0.351165	
	O33	2.552	1.65	0.4	0.104874	
	O78	2.612	1.65	0.4	0.090265	1.624355
Cu3	O24	1.9843	1.65	0.4	0.433549	
	O24	1.9843	1.65	0.4	0.433549	
	N9	2.01	1.61	0.4	0.367879	
	N9	2.01	1.61	0.4	0.367879	
	O1W	2.3309	1.65	0.4	0.182273	1.78513
Cu4	O22	1.9857	1.65	0.4	0.432034	
	O22	1.9857	1.65	0.4	0.432034	
	N10	2.0022	1.61	0.4	0.375123	
	N10	2.0022	1.61	0.4	0.375123	

	O5W	2.3178	1.65	0.4	0.188341	1.802657
Cu6	O4	1.9086	1.65	0.4	0.523876	
	O4	1.9086	1.65	0.4	0.523876	
	O3W	1.9869	1.65	0.4	0.43074	
	O3W	1.9869	1.65	0.4	0.43074	
	O2W	2.232	1.65	0.4	0.2334	2.142633
Cu7	N17	1.9531	1.61	0.4	0.424115	
	N15	1.975	1.61	0.4	0.401519	
	N14	1.9756	1.61	0.4	0.400917	
	N16	2.1266	1.61	0.4	0.274858	
	O31	2.511	1.65	0.4	0.116193	
	O35	2.752	1.65	0.4	0.063609	1.681212
Cu5	O41	1.9391	1.65	0.4	0.485416	
	N12	1.9514	1.61	0.4	0.425922	
	O36	2.0325	1.65	0.4	0.384331	
	N13	2.0869	1.61	0.4	0.303538	
	O7W	2.672	1.65	0.4	0.077692	1.676898

As shown in Table S2 and Table S4, BVS calculations of Cu atoms in the compounds **1** and **2** have been performed, the values of Cu atoms in compound **1** are 1.703, 1.611, 1.681, 1.764, 1.807, respectively, while the values of Cu atoms in compound **2** are 1.676, 1.624, 1.803, 2.142, 1.681, 1.677, respectively, which indicates that the valence states are about +2 for all Cu atoms in both of two compounds.

Table S5 Bond lengths and valence band summations of protonated oxygens in 2.

Atom1	Atom2	Rij	Ro	B	Sij	SUM
O3	Nb26	1.9576	1.921	0.319	0.891604	
	Nb12	2.3019	1.921	0.319	0.302994	
	Nb13	2.3200	1.921	0.319	0.28622	1.480878

Table S6 Hydrolytic catalysis of chemical warfare agent simulants (DMMP and DECP) by PONbs.

Compound	Substrate (DMMP or DECP)	Conver-sion	Ref
$K_{12}[Ti_2O_2][SiNb_{12}O_{40}]\cdot 22H_2O$	DMMP	35.5%	[7]
$K_{12}[Ti_2O_2][GeNb_{12}O_{40}]\cdot 19\ H_2O$	DMMP	54%	[7]
$H_2Li_5Na_5K_5[Cu(en)_2]_7[Nb_{47}O_{128}(OH)_6(CO_3)_2]\cdot 20H_2O$	DMMP	46%	[23]
$H_{16}K_{24}Na_{26}[Cu_3(en)_6][(\beta\text{-}H_4Nb_{52}O_{150})_2]\cdot 88H_2O$	DMMP	23.66%	[22]
$Na_{12}\{H_{24}NbO_8Cu_{24}I_3O_3\{[Nb_7(OH)O_{21}]_8\}\cdot 34H_2O$	DMMP	26.5%	S3
$Na_{12}(H_2O)_{22}\{H_{22}NbO_8Cu_{24}I_5O[Nb_7(OH)O_{21}]_8\}\cdot 34H_2O$	DMMP	20.63%	S3

$Na_2\{H_{34}GdO_8Cu_{24}Br_5O[Nb_7(OH)O_{21}]_8\}\cdot 12H_2O$	DMMP	19.35%	S3
$H_4Na_8K_6[Sb_2Nb_{24}O_{72}]\cdot 30H_2O$	DMMP	35.9%	[34]
1	DMMP	40%	This work
$K_{12}[Ti_2O_2][GeNb_{12}O_{40}]\cdot 19\ H_2O$	DECP	100% (30 min)	[7]
$K_{12}[Ti_2O_2][SiNb_{12}O_{40}]\cdot 22\ H_2O$	DECP	100% (30 min)	[7]
$K_8Nb_6O_{19}$	DECP	90% (30 min)	[7]
$H_{13}[(CH_3)_4N]_{12}[PNb_{12}O_{40}(V^{V}O)_2(V^{IV}{}_4O_{12})_2]\cdot 22H_2O$	DECP	98% (30 min)	[8]
$Na_{15}[PNb_{12}O_{40}]$	DECP	95% (30 min)	[8]
$[C_{18}H_{37}N(CH_3)_3]_7HNb_6O_{19}$	DECP	100% (2 h)	S4
Mg_3Al-LDH-Nb_6 composite	DECP	97% (30 min)	S5
$Na_{12}\{H_{24}NbO_8Cu_{24}I_3O_3\{[Nb_7(OH)O_{21}]_8\}\cdot 34H_2O$	DECP	100% (35 min)	S3
$Na_{12}(H_2O)_{22}\{H_{22}\{NbO_8Cu_{24}I_5O[Nb_7(OH)O_{21}]_8\}\cdot 34H_2O$	DECP	100% (20 min)	S3
$Na_2\{H_{34}GdO_8Cu_{24}Br_5O[Nb_7(OH)O_{21}]_8\}\cdot 12H_2O$	DECP	100% (30 min)	S3
1	DECP	100% (30 min)	This work

Section S3 Additional Figures and Characteristics

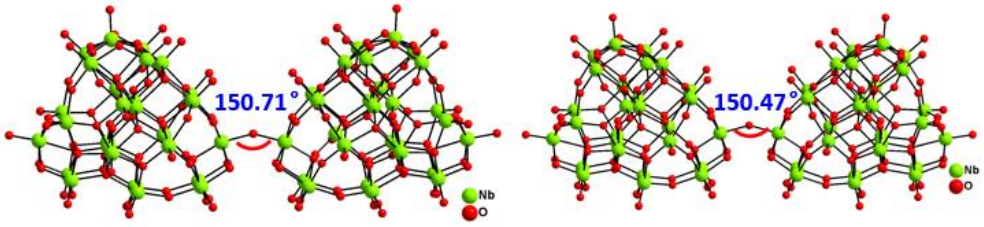

(a) **(b)**

Fig. S1 The ∠Nb-O-Nb angles of $\{Nb_{54}O_{151}\}$ cluster in **1** (a) and **2** (b).

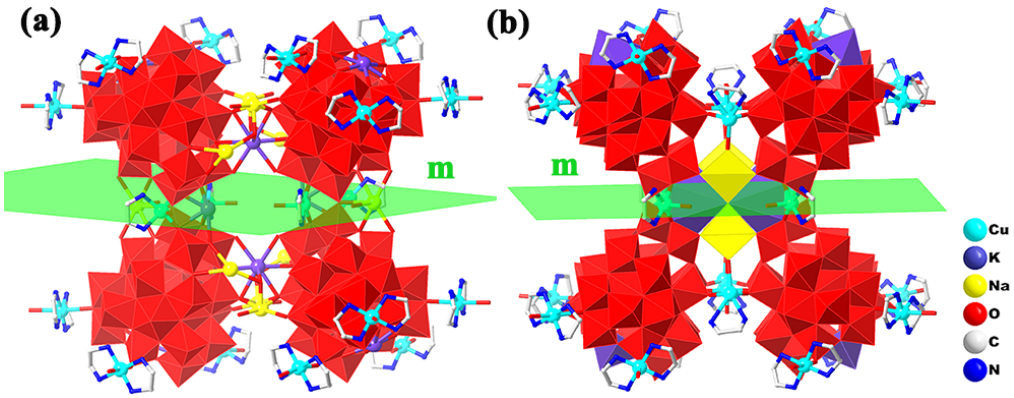

Fig. S2 View of *m* plane in **1** (a) and **2** (b), respectively.

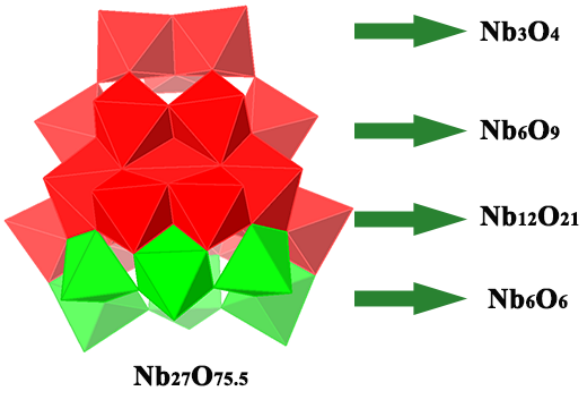

Fig. S3 View of the Nb_3O_4, Nb_6O_9, $Nb_{12}O_{21}$, Nb_6O_6 motifs in $Nb_{27}O_{75.5}$ cluster.

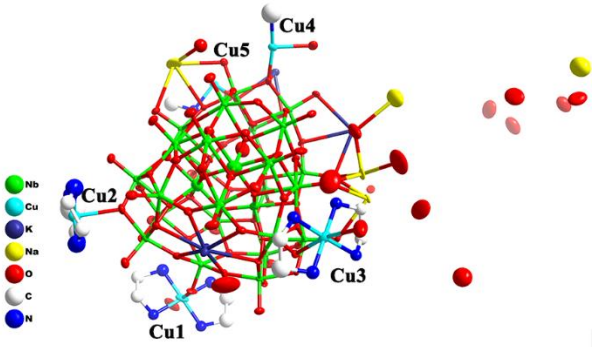

Fig. S4 Asymmetric unit of **1** represented by ORTEP plot.

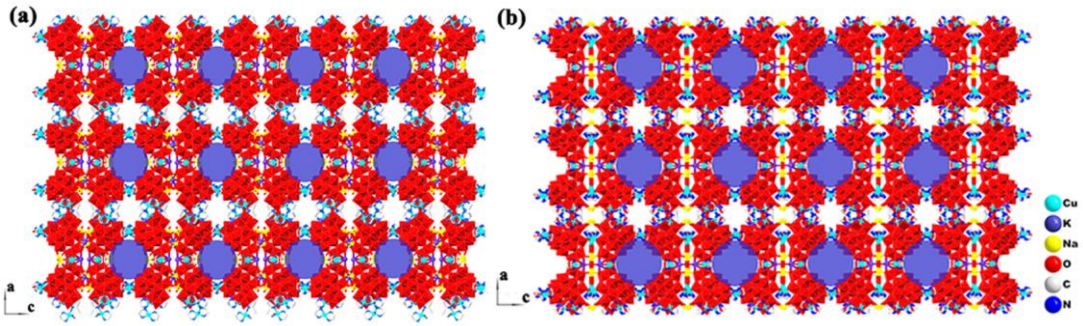

Fig. S5 View of the 3D stacking structures of **1**(a) and **2** (b) along the *b*-axis.

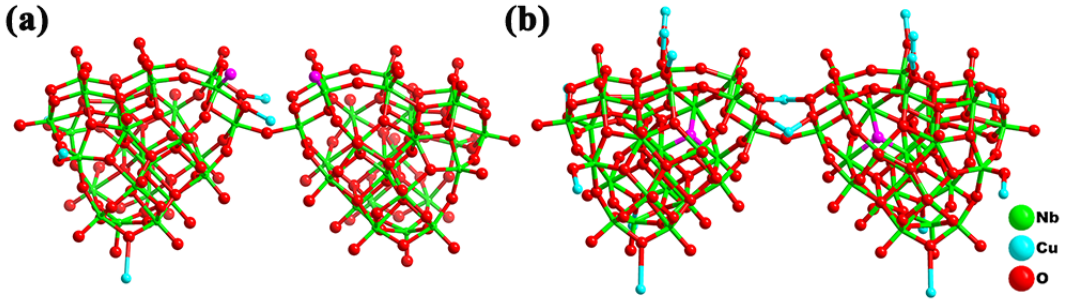

Fig. S6 The protonated oxygen atoms in **1** (a) and **2** (b). Color code: protonated oxygen, purple.

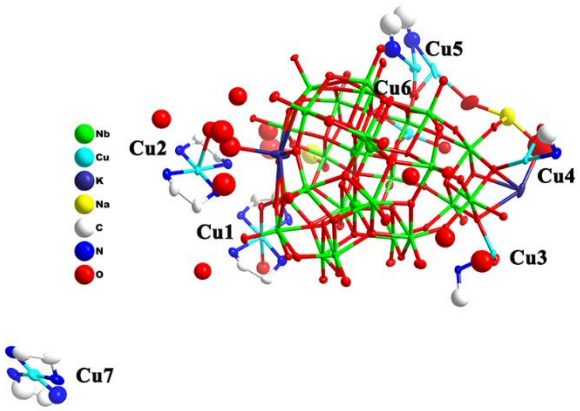

Fig. S7 Asymmetric unit of **2** represented by ORTEP plot.

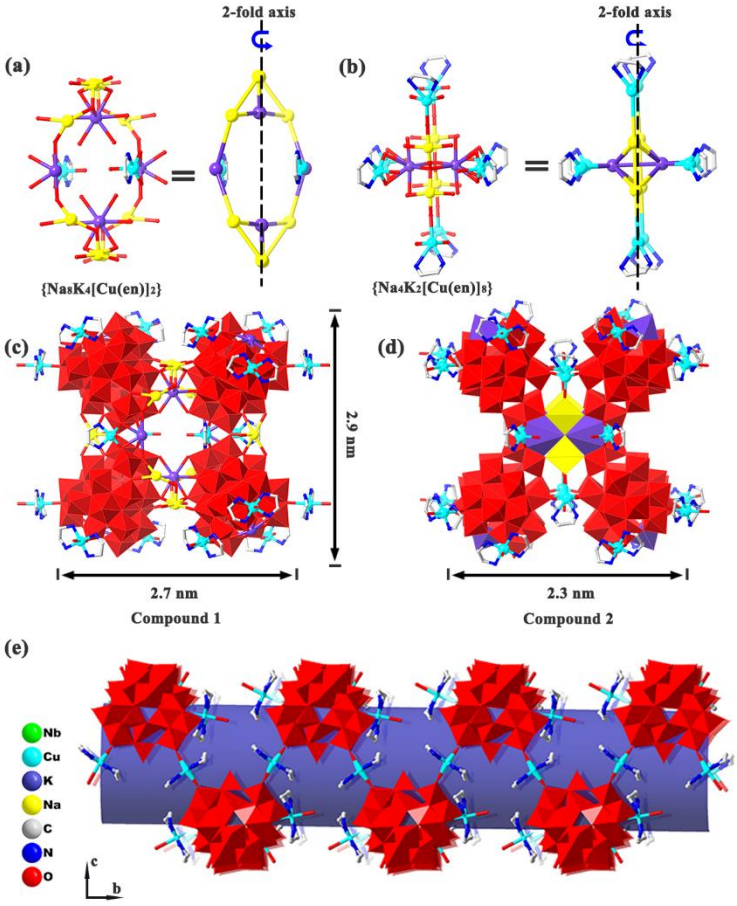

Fig. S8 The structures of compounds **1** and **2**. (a) $\{Na_8K_4[Cu(en)]_2\}$ cage and linkage between alkaline metals in **1**; (b) $\{Na_4K_2[Cu(en)]_8\}$ cage and linkage between alkaline metals in **2**; (c) the dimer $\{Nb_{108}O_{302}\}$ of **1**; (d) the dimer $\{Nb_{108}O_{302}\}$ cluster of **2**; (e) the nanotube in **1** (omitted all of alkaline metals), viewed along [100] direction, the unique $\{Nb_{54}O_{151}\}$ SBUs combined with copper-amine complexes in parallel direction. Red polyhedrons: NbO_6.

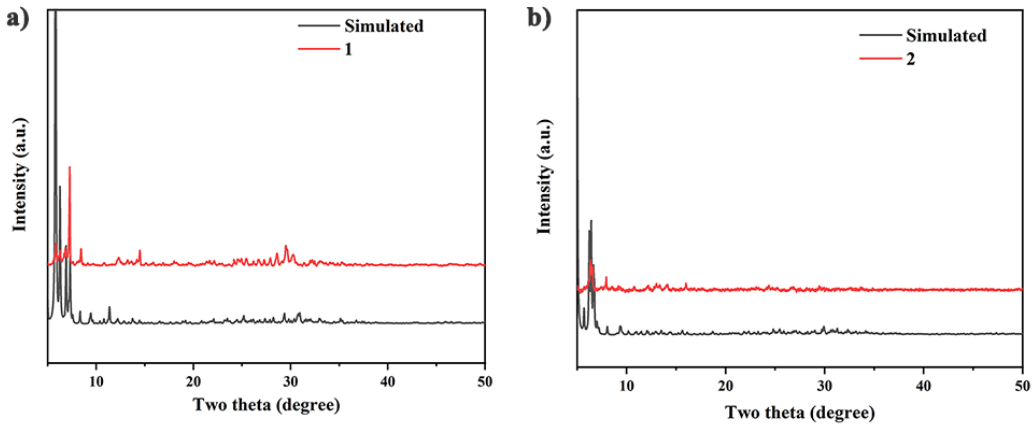

Fig. S9 The simulated and experimented PXRD patterns of of **1** and **2**.

As shown in Fig. S9, I have tried to grind down the samples as fine as possible and re-test the PRXD of two compounds, and as shown in Fig S9, The main experimental PXRD peaks of two compounds are consistent with their simulated ones, respectively, except that there are differences in intensity, which may be due to the anisotropy of crystals.

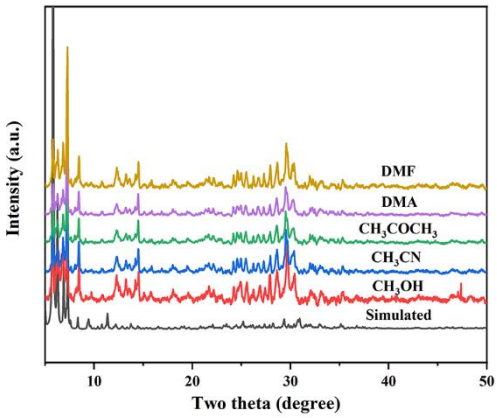

Fig. S10 The simulated and PXRD patterns of **1** after being soaked in different organic solvents.

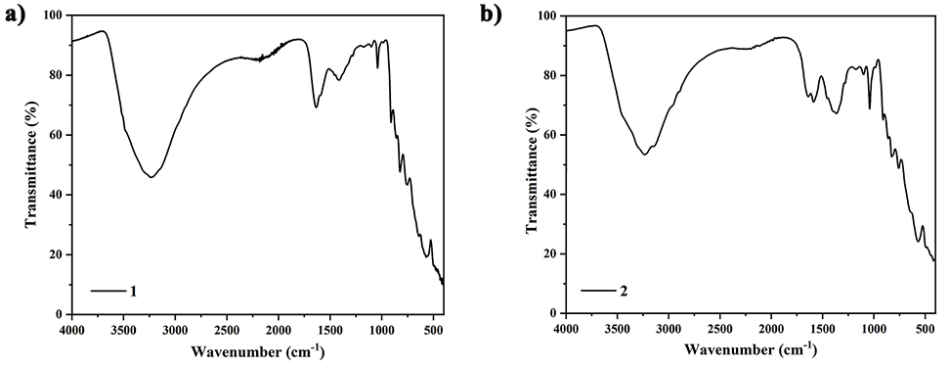

Fig. S11 IR spectra of **1** and **2**.

As shown in Fig. S11, in the low wavenumber range, four main typical vibration peaks appear at 469-831 cm^{-1}, which are assigned to the stretching vibrations of bridging Nb-O_b-Nb, Cu-O and Cu-N. [S6, S7] Four strong peaks at 846-1036 cm^{-1}, are attributed to the vibration of the terminal Nb=O_t.

[S8, S9] Peaks between 1101 and 1641 cm^{-1} are ascribed to the vibration of the C–N. [S6] In the high wavenumber region, the strong and wide peak between 3000 cm^{-1} and 3500 cm^{-1} corresponds to the O–H stretching vibration of lattice and coordination water molecules. [S10] These results are in good agreement with the result of the X-ray single-crystal structural analysis.

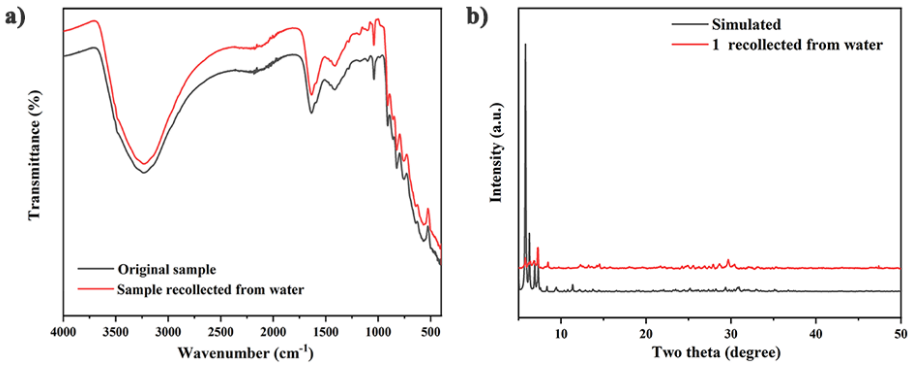

Fig. S12 IR and PXRD spectra of **1** before and after being soaked in water.

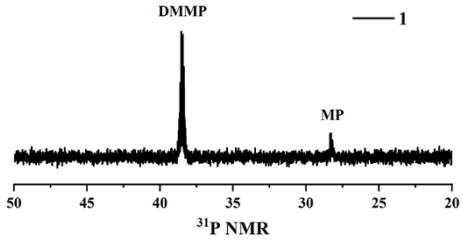

Fig. S13 ^{31}P NMR peaks of DMMP and MP in 48h of **1**.

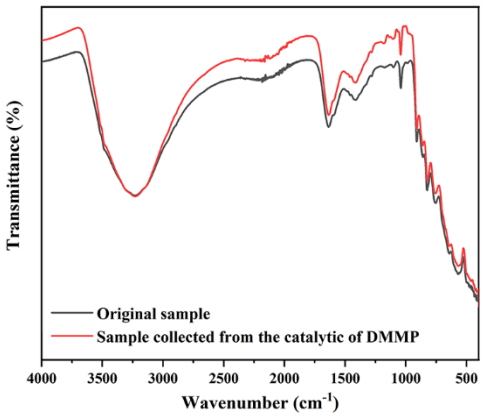

Fig. S14 IR spectra of **1** before and after catalytic hydrolysis of DMMP.

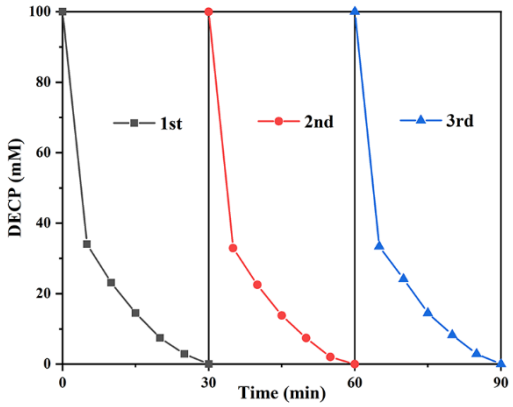

Fig. S15 Three-cycle conversions of DECP to DEHP versus reaction time of using catalyst **1**.

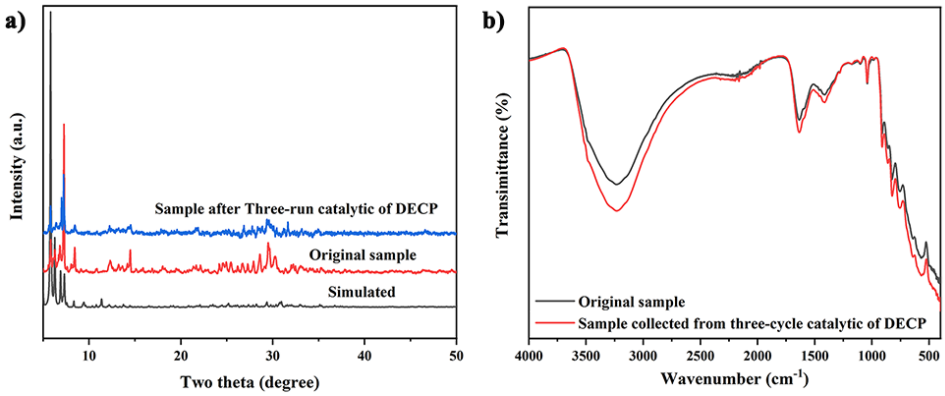

Fig. S16 XRD patterns and IR spectra before and after three-cycle catalytic hydrolysis of DECP by **1**.

As shown in Fig.S16, the changes between the PXRD after the catalytic cycles and original samples are that the PXRD lines become rougher but the main peaks are accordance with the original samples, which may due to the worse crystallinity and decrease of quantity of catalyst after the catalytic cycles.

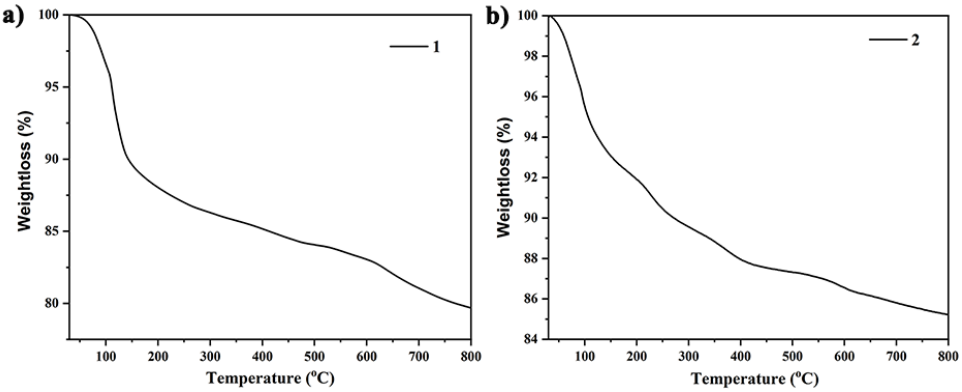

Fig. S17 TG curves of **1** and **2**.

As shown in Fig. S17, both of **1** and **2** experienced a continuous weight loss process in the temperature range of 30 °C to about 600 °C. The first weight loss stage that occurs when the temperature was within the temperature range of 30 °C to 120 °C should be ascribed to the loss of lattice water molecules. Based on the first weight loss, 27 and 22 lattice water molecules were added

for **1** and **2**, respectively.

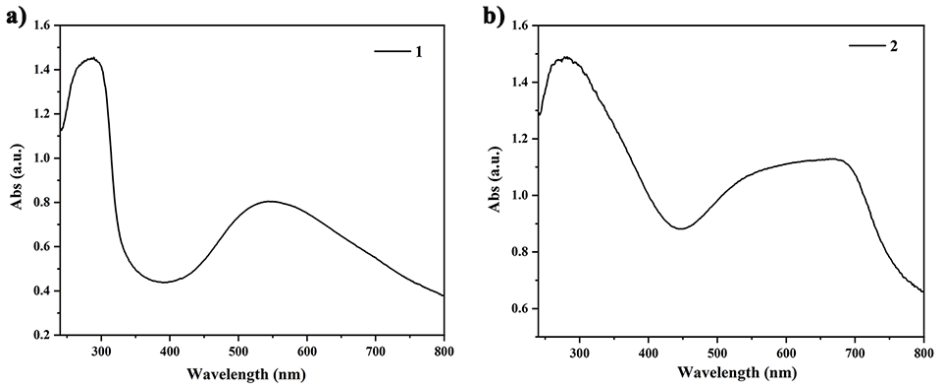

Fig. S18 UV-vis Spectra of **1** and **2**.

The UV diffuse spectra of **1** and **2** are determined in the range of 240 to 800 nm. The absorption peak in the range of 240 to 400 nm can be ascribed to the charge transfer of O→Nb. The broad absorption peak in the range of 400 to 800 nm can be attributed to d-d transfers of Cu^{2+}.

Section S4: References

[S1] M. FILOWITZ, R. K. C. HO, W. G. KLEMPERER, and W. SHUM, *Inorg. Chem.*, 1979, **18**, 93-103.

[S2] G. M. Sheldrick, *SHELXL97*, Program for Crystal Structure Refinement, University of Gottingen: Gottingen, Germany, 1997.

[S3] Y. L. Wu, R. T. Zhang, Y. Q. Sun, X. X. Li and S. T. Zheng, *Front. Chem.*, 2020, 8, 586009.

[S4] X. Q. Li, J. Dong, H. F. Liu, X. R. Sun, Y. N. Chi, C. W. Hu, *J. Hazard. Mater.*, 2018, **344**, 994-999.

[S5] J. Dong, H. J. Lv, X. R. Sun, Y. Wang, Y. M. Ni, B. Zou, N. Zhang, A. X. Yin, Y. N. Chi, and C. W. Hu, *Chem. Eur. J.*, 2018, **24**,19208-19215.

[S6] J. Q. Shen, Y. Zhang, Z. M. Zhang, Y.G. Li, Y. Q. Gao and E. B. Wang, *Chem. Commun*., 2014, **50**, 6017-6019.

[S7] M. Nyman, F. Bonhomme, T. M. Alam, M. A. Rodriguez, B. R. Cherry, J. L. Krumhansl, T. M. Nenoff, and A. M. Sattler, *Science*., 2012, **297**, 996-998.

[S8] G. Guo, Y. Xu, J. Cao and C. Hu, *Chem. Eur. J.*, 2012, **18**, 3493-3497.

[S9] J. H. Son, C. A. Ohlin, R. L. Johnson, P. Yu and W. H. Casey, *Chem. Eur. J.*, 2013, **19**, 5191-5197.

[S10] R. Chris, B. Valérie, G. M. Evan, R. Christian, B. Colette, *Inorg. Chem.*, 2012, **51**, 1142-1151.